A novel weighted density functional theory for adsorption, fluid-solid interfacial tension, and disjoining properties of simple liquid films on planar solid surfaces

Yang-Xin Yu[a)]
Department of Chemical Engineering, Tsinghua University, Beijing 100084, People's Republic of China and State Key Laboratory of Chemical Engineering, Tsinghua University, Beijing 100084, People's Republic of China

(Received 12 March 2009; accepted 18 June 2009; published online 14 July 2009)

A novel weighted density functional theory (WDFT) for an inhomogeneous 12-6 Lennard-Jones fluid is proposed based on the modified fundamental measure theory for repulsive contribution, the mean-field approximation for attractive contribution, and the first-order mean-spherical approximation with a weighted density for correlation contribution. Extensive comparisons of the theoretical results with molecular simulation and experimental data indicate that the new WDFT yields accurate density profiles, adsorption isotherms, fluid-solid interfacial tensions, as well as disjoining potentials and pressures of simple gases such as argon, nitrogen, methane, ethane, and neon confined in slitlike pores or near graphitic solid surfaces. The present WDFT performs better than the nonlocal density functional theory, which is frequently used in the study of adsorption on porous materials. Since the proposed theory possesses a good dimensional crossover and is able to correctly reduce to two-dimensional case, it performs very well even in very narrow pores. In addition, the present WDFT reproduces very well the supercritical fluid-solid interfacial tensions, whereas the theory of Sweatman underestimates them at high bulk densities. The present WDFT predicts that the increase in the fluid-wall attraction may change the sign of the interfacial tension and hence may make the wall from "phobic" to "philic" with respect to the fluid. The new WDFT is computationally as simple and efficient as the mean-field theory and avoids the second-order direct correlation function as an input. It provides a universal way to construct the excess Helmholtz free-energy functional for inhomogeneous fluids such as Yukawa, square-well, and Sutherland fluids. © *2009 American Institute of Physics*. [DOI: 10.1063/1.3174928]

I. INTRODUCTION

The interfacial phenomena such as adsorption, wetting, prewetting, and thin film on solid surface, which are a result of the interplay between fluid and solid substrates, are widely found in industrial processes and nature. They play an important role in adsorptive separation, gas storage, protective coatings and paints, nanoscale patterning, and structure fabrication.[1] To understand these phenomena, it is necessary to obtain the quantitative dependence of the interfacial properties (e.g., adsorption, interfacial tension, disjoining potential, and pressure) on the strengths and ranges of the fluid-fluid and fluid-substrate interactions. Although attempts have been carried out to solve this problem using molecular simulations,[2–5] integral equations,[6] and DFTs,[7–17] a simple but accurate theoretical method is still under pursuing by the scientists in this research field. Among the above three approaches, density functional theory (DFT) is the most promising in the description of the interfacial properties.[18]

It is well known that the Lennard-Jones (LJ) potential, which represents a basic intermolecular force between any two real simple molecules, is very important in statistical thermodynamics. The LJ potential is given by[19]

$$u^{\mathrm{LJ}}(r) = 4\varepsilon\left[\left(\frac{\sigma}{r}\right)^{12} - \left(\frac{\sigma}{r}\right)^{6}\right], \tag{1}$$

where σ and ε stand for the size and energy parameters of the LJ potential, respectively. In principle, any successful statistical mechanic theory should describe both the homogeneous and inhomogeneous LJ fluids accurately. Early theories including van der Waals square-gradient theory[20] are useful for weakly inhomogeneous systems such as the interface of a vapor-liquid coexistence.[21] A mean-field theory (MFT) is not adequate for the description of fluid-solid interfaces. Thus, Katsov and Weeks[22] modified the MFT and approximated the structure of the nonuniform LJ system by that of a hard-sphere fluid in an appropriately chosen effective reference field comprised of two parts: a bare external field from the hard-core solute and a much more slowly varying part describing the unbalanced attractive interactions. Later, the hard-core interaction was replaced by the more realistic soft repulsive force.[23] Most applications of MFT in surface problems are a combination of weighted density functional for the short-ranged repulsion and the MFT for long-ranged attractions.[8,24,25] In general, the short-ranged repulsion is represented by an effective hard-core interaction.[26,27] It proves that among various versions of weighted density functional theories (WDFTs) for inhomo-

[a)]Electronic mail: yangxyu@mail.tsinghua.edu.cn.

geneous hard-sphere fluids, the modified fundamental measure theory[28–30] (MFMT) is the most successful one and it has been widely applied as a reference part of the Helmholtz free-energy functional.[25]

Several types[10,12,16,31–34] of DFT for the LJ fluid have been reported in literature but, in general, they can be divided into three categories: full perturbative, partial perturbative, and weighted density approaches. In the fully perturbative approach, the Helmholtz free-energy functional is evaluated through a functional Taylor expansion around the corresponding bulk fluid.[9,33,35] In order to obtain sufficient accuracy, the terms containing at least the third-order direct correlation function (DCF) need to be taken into account. Choudhury and Ghosh[9] evaluated the third-order DCF at a suitable weighted density to include the effect of a subset of the higher order terms. In the partial perturbative approach, the Helmholtz free-energy functional comprises the hard-sphere part from a weighted density functional approximation and a long-ranged attractive part from the functional Taylor expansion.[13,15,16] Since the WDFT is used for the reference fluid, the functional Taylor expansion of the excess Helmholtz free-energy functional converges more rapidly. In most cases, a good agreement with molecular simulation is obtained when the expansion is truncated at the second-order DCF term.[15,16] Obviously the partial perturbative approach is more efficient than the full perturbative one. Regretfully, the DCF of bulk fluid is required as an input in both perturbative approaches whereas the DCF is not available in some cases. In the weighted density functional approach, the Helmholtz free-energy functional due to both short-ranged repulsion and long-ranged dispersion are determined in terms of the weighted densities.[10,11,32,36–38]

The significant difference between various WDFTs is the form of the weight function used to define a smoothed density. The weight function can be determined from the interpolation between the exact low density limit and a mean-field weight function equal to the normalized attractive potential,[36] from the accurate pair DCF for a uniform fluid,[32] or from a FMT.[37] Recently, we found that the exact low density limit has little effect on adsorption and phase transition in pores, and thus proposed a mean-field-type weight function for the confined LJ fluid. The theory reproduces surface tension, adsorption, and capillary condensation in not very narrow pores very well.[10,11] It should also be mentioned that Schmidt[37] proposed a so-called soft fundamental measure theory (SFMT), which was built on well-defined limiting cases, i.e., the virial expansion and the zero-dimensional limit, where the behavior of the exact free-energy functional is known. The SFMT works best for potentials that are sufficiently short ranged but cannot tackle true long-ranged potentials such as the Coulomb or inverse-power potential with small exponents.

From our experience on DFT, the hard-sphere part of the Helmholtz free-energy functional for the LJ fluid contributes a lot to the density profile and adsorption at high bulk densities, while the attractive part dominates at low bulk densities. If a DFT reduces to an accurate equation of state at bulk limit, the prediction of phase transition in confined space is good. Moreover the combination of the MFMT with the MFT is able to give an accurate density distribution and adsorption when the effect of bulk equation of state is neglected. Therefore, in this work I propose a new WDFT where the excess Helmholtz free-energy functional comprises a hard-core contribution from the MFMT, an attractive contribution from the MFT, and a correlation contribution obtained from an accurate bulk equation of state for the LJ fluid with a weighted density. The new WDFT not only avoids using the DCF of bulk fluid as an input but also predicts the structures of the LJ fluid. The performance of the proposed WDFT is examined extensively by comparing with the existing molecular simulation and experimental data for density profiles, adsorption, fluid-solid interfacial tensions, and disjoining properties of a liquid thin film on a planar solid surface.

II. DENSITY FUNCTIONAL THEORY

In statistical mechanics, the grand potential $\Omega[\rho(\mathbf{r})]$ of an inhomogeneous fluid is related to the Helmholtz free-energy functional via a Legendre transform,[7]

$$\Omega[\rho(\mathbf{r})] = F[\rho(\mathbf{r})] + \int \rho(\mathbf{r})[\psi^{\text{ext}}(\mathbf{r}) - \mu]d\mathbf{r}, \tag{2}$$

where $F[\rho(\mathbf{r})]$ is the Helmholtz free-energy functional, $\psi^{\text{ext}}(\mathbf{r})$ is the external potential, and μ is the fluid chemical potential which is obtained from the bulk density ρ_b. The Helmholtz free-energy functional can be formally expressed as an ideal-gas (id) contribution plus an excess term that can be further decomposed in hard-core (hs), attractive (att), and correlation (cor) contributions, i.e.,

$$F[\rho(\mathbf{r})] = F^{\text{id}} + F^{\text{hs}} + F^{\text{att}} + F^{\text{cor}}. \tag{3}$$

The ideal-gas contribution to the Helmholtz free-energy functional is exactly known as

$$F^{\text{id}} = k_B T \int \rho(\mathbf{r})\{\ln[\rho(\mathbf{r})\Lambda^3] - 1\}d\mathbf{r}, \tag{4}$$

where T is the absolute temperature, k_B is Boltzmann constant, and Λ is the de Broglie wavelength.

For a hard-sphere fluid without disperse interactions, the MFMT developed by Yu *et al.*[28,29] is the most accurate and thus it is selected in this work,

$$F^{\text{hs}} = k_B T \int [\Phi^{\text{hs}(S)} + \Phi^{\text{hs}(V)}]d\mathbf{r}, \tag{5}$$

where $\Phi^{\text{hs}(S)}$ and $\Phi^{\text{hs}(V)}$ are the scalar and vector parts of reduced excess Helmholtz free-energy density due to hard-core repulsion, respectively. According to the MFMT,[28–30] they are given by

$$\Phi^{\text{hs}(S)} = -n_0 \ln(1-n_3) + \frac{n_1 n_2}{1-n_3} + \frac{n_2^3}{36\pi n_3^2}\ln(1-n_3) + \frac{n_2^3}{36\pi n_3(1-n_3)^2}, \tag{6}$$

$$\Phi^{\mathrm{hs}(V)} = -\frac{\mathbf{n}_{V1}\cdot\mathbf{n}_{V2}}{1-n_3} - \frac{n_2\mathbf{n}_{V2}\cdot\mathbf{n}_{V2}}{12\pi n_3^2}\ln(1-n_3) - \frac{n_2\mathbf{n}_{V2}\cdot\mathbf{n}_{V2}}{12\pi n_3(1-n_3)^2}, \tag{7}$$

where $n_\alpha(\mathbf{r})$ (α=1, 2, 3, $V1$, and $V2$) are the hard-sphere weighted densities defined by

$$n_\alpha(\mathbf{r}) = \int \rho(\mathbf{r}')w^{(\alpha)}(|\mathbf{r}'-\mathbf{r}|)d\mathbf{r}'. \tag{8}$$

At bulk homogeneous limit, the vector weighted densities vanish and the excess Helmholtz energy density $\Phi^{\mathrm{hs}(S)}+\Phi^{\mathrm{hs}(V)}$ becomes identical to that from the Boublik–Mansoori–Carnahan–Starling–Leland equation of state.[39] In Eq. (8), the weight functions $w^{(\alpha)}(r)$ (α=1, 2, 3, $V1$, and $V2$) are expressed in terms of the Dirac delta function $\delta(r)$ and the Heaviside step function $\theta(r)$,[34,40]

$$w^{(2)}(r) = \pi d^2 w^{(0)}(r) = 2\pi d w^{(1)}(r) = \delta(d/2-r), \tag{9}$$

$$w^{(3)}(r) = \theta(d/2-r), \tag{10}$$

$$w^{(V2)}(\mathbf{r}) = 2\pi d w^{(V1)}(\mathbf{r}) = (\mathbf{r}/r)\delta(d/2-r), \tag{11}$$

where d is the effective hard-sphere diameter of the fluid. For systems with special symmetry, Eq. (8) can be expressed more explicitly according to the nature of the density distribution. These expressions have been documented elsewhere.[28]

In a system with only attractive interaction, the mean-field approximation is a good choice to consider the attractive contribution to the Helmholtz free-energy functional. In the MFT, I have

$$F^{\mathrm{att}} = \frac{1}{2}\int d\mathbf{r}'\int d\mathbf{r}\rho(\mathbf{r}')\rho(\mathbf{r})u^{\mathrm{att}}(|\mathbf{r}'-\mathbf{r}|), \tag{12}$$

where $u^{\mathrm{att}}(r)$ is the attractive part of potential between two interacting particles. Alternatively, F^{att} can be obtained from a mean-field weighted density proposed by Peng and Yu.[10,11]

When the intermolecular potential contains both repulsive and attractive interactions, a correlation term of Helmholtz free-energy functional should be considered. Previous DFTs, either perturbative ones or weighted density ones, use the pair-DCF $C^{(2)}(r)$ as an input to include the correlation term. These DFTs are accurate for the inhomogeneous supercritical fluids. However, the analytical expression of DCF is not available in most cases. In this work, I propose a new way to develop the Helmholtz free-energy functional due to correlation effect in terms of weighted density defined as

$$\bar{\rho}(\mathbf{r}) = \int \rho(\mathbf{r}')w^{(\mathrm{cor})}(|\mathbf{r}'\text{-}\mathbf{r}|)d\mathbf{r}', \tag{13}$$

where $w^{(\mathrm{cor})}(r)$ is the correlation weight function given by

$$w^{(\mathrm{cor})}(r) = \theta(d-r)/(4\pi d^3/3). \tag{14}$$

Subsequently, the Helmholtz free-energy functional due to the correlation effect can be expressed as

$$F^{\mathrm{cor}} = k_B T\int \bar{\rho}(\mathbf{r})f^{\mathrm{cor}}[\bar{\rho}(\mathbf{r})]d\mathbf{r}, \tag{15}$$

where f^{cor} is the reduced Helmholtz free-energy per particle due to the correlation effect when the bulk density is replaced by weighted density $\bar{\rho}(\mathbf{r})$. It can be obtained from any existing equation of state. As an example, I use the first-order mean-spherical approximation (FMSA) for the LJ fluid.[41] In the FMSA, the LJ potential is approximated according to the Barker–Henderson theory,[26] i.e.,

$$u(r) = \begin{cases} \infty & (r<d) \\ 0 & (d<r\le\sigma) \\ u^{\mathrm{att}}(r) & (\sigma<r\le r_c) \\ 0 & (r>r_c), \end{cases} \tag{16}$$

where $u^{\mathrm{att}}(r)$ is given by

$$u^{\mathrm{att}}(r) = \begin{cases} 0 & (r\le\sigma) \\ 4\varepsilon\left[\left(\frac{\sigma}{r}\right)^{12}-\left(\frac{\sigma}{r}\right)^{6}\right] & (\sigma<r\le r_c) \\ 0 & (r>r_c) \end{cases} \tag{17}$$

when only a truncated LJ potential is used. As usual, r_c is the cutoff distance. The effective hard-sphere diameter d is derived by Barker and Henderson,[26]

$$d = \int_0^\sigma [1-e^{-\beta u^{\mathrm{rep}}(r)}]dr, \tag{18}$$

where $\beta=1/k_BT$. From Eq. (18) one can find that d is a function of temperature. When the reduced temperature $T^*=k_BT/\varepsilon=0\sim15$, d can be accurately reproduced by[42]

$$\frac{d}{\sigma} = \frac{1+0.2977T^*}{1+0.331\,63T^*+1.0477\times10^{-3}T^{*2}}. \tag{19}$$

The excess Helmholtz free-energy per particle due to correlation effect is then obtained from

$$f^{\mathrm{cor}} = f_1 + f_2 - f^{\mathrm{MF}}, \tag{20}$$

where f^{MF} is the mean-field term which can be obtained from Eqs. (12) and (17) by setting $r_c=\infty$,

$$f^{\mathrm{MF}} = -(16/9)\pi\beta\varepsilon\rho\sigma^3, \tag{21}$$

where ρ is the density. f_1 and f_2 are the FMSA expansion terms of T^{*-1} and T^{*-2}, respectively. Tang and Lu[41] derived the explicit expression of f_1 and f_2. I reformulate their expressions as follows:

$$f_1 = -12\eta\sum_{i=1}^{2}\left[\frac{\beta\varepsilon_i L(\lambda_i)}{(1-\eta)^2Q(\lambda_i)\lambda_i^2} - \frac{\beta\varepsilon_i(1+\lambda_i)}{\lambda_i^2}\right] + 48\eta\beta\varepsilon\left[\frac{1}{9}\left(\frac{\sigma}{d}\right)^{12}-\frac{1}{3}\left(\frac{\sigma}{d}\right)^{6}\right] - 48\eta\beta\varepsilon g^{\mathrm{hs}}(d)\left[\frac{1}{9}\left(\frac{\sigma}{d}\right)^{12}-\frac{1}{3}\left(\frac{\sigma}{d}\right)^{6}+\frac{2}{9}\left(\frac{\sigma}{d}\right)^{3}\right], \tag{22}$$

$$f_2 = -6\eta \sum_{i=1}^{2}\sum_{j=1}^{2} \frac{\beta^2 \varepsilon_i \varepsilon_j}{(\lambda_i+\lambda_j)Q^2(\lambda_i)Q^2(\lambda_j)} - 24\eta\beta^2\varepsilon \sum_{i=1}^{2} \frac{\varepsilon_i}{Q^2(\lambda_i)}\left[\frac{1}{9}\left(\frac{\sigma}{d}\right)^{12} - \frac{1}{3}\left(\frac{\sigma}{d}\right)^{6} + \frac{2}{9}\left(\frac{\sigma}{d}\right)^{3}\right], \tag{23}$$

where $\eta=\pi\rho d^3/6$ is the packing fraction and $g^{\mathrm{hs}}(d)$ is the radial distribution function of hard-sphere fluid at contact, which is derived from the Carnahan–Starling equation of state,

$$g^{\mathrm{hs}}(d) = (1-\eta/2)/(1-\eta)^3. \tag{24}$$

The functions $L(t)$ and $Q(t)$ in Eqs. (22) and (23) are defined by

$$L(t) = (1+\eta/2)t + 1 + 2\eta, \tag{25}$$

$$Q(t) = \frac{S(t) + 12\eta L(t)e^{-t}}{(1-\eta)^2 t^3}, \tag{26}$$

where

$$S(t) = (1-\eta)^2 t^3 + 6\eta(1-\eta)t^2 + 18\eta^2 t - 12\eta(1+2\eta). \tag{27}$$

In Eqs. (25)–(27), $t=\lambda_1$ or λ_2. λ_i and ε_i ($i=1$ and 2) are the potential parameters for the hard-core two-Yukawa potential used to mimic the LJ fluid. For the LJ fluid, their values are taken as $\lambda_1=2.9637d/\sigma$, $\lambda_2=14.0167d/\sigma$, $\varepsilon_1=k_0e^{\lambda_1(\sigma/d-1)}$, $\varepsilon_2=-k_0e^{\lambda_2(\sigma/d-1)}$, and $k_0=2.1717\sigma/d$.

Once the expression of the Helmholtz free-energy functional is determined, the minimization of the grand potential with respect to the density profile yields the Euler–Lagrange equation

$$\ln \rho(\mathbf{r}) = \beta\left[\mu - \frac{\delta(F^{\mathrm{hs}}+F^{\mathrm{att}}+F^{\mathrm{cor}})}{\delta\rho(\mathbf{r})} - \psi^{\mathrm{ext}}(\mathbf{r})\right]. \tag{28}$$

The chemical potential μ at bulk density ρ_b is obtained by switching off the external potential and the density distribution $\rho(\mathbf{r})$ is solved from Eq. (28) using the Picard-type iterative method. In this work, I refer the calculated density profiles and adsorption isotherms as the results of the MFT when I neglect F^{cor} (i.e., $F^{\mathrm{cor}}=0$). From the comparison of the equation used, one can find that the present WDFT is almost as computational efficient as the MFT and simpler in form than the WDFT reported in literature.[32]

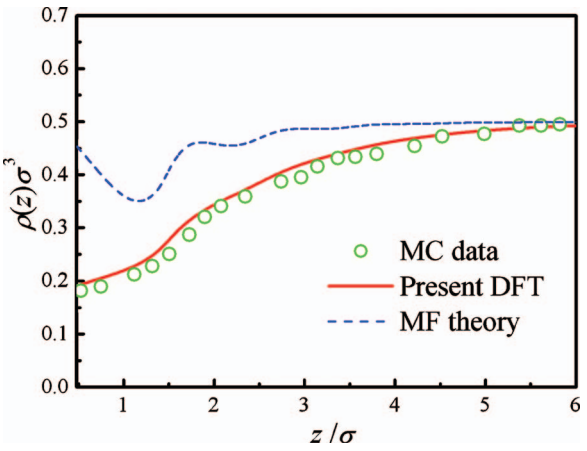

FIG. 1. Density profiles of LJ fluid near a hard wall at bulk density of $\rho_b\sigma^3=0.5$ and reduced temperature of $T^*=1.35$. The circles, dashed, and solid lines represent the results from the MC simulations (Ref. 43), MFT, and present WDFT, respectively.

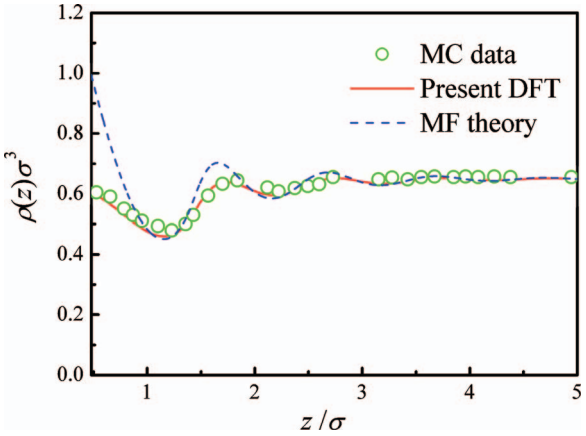

FIG. 2. Same as in Fig. 1 but at a moderate bulk density of $\rho_b\sigma^3=0.65$.

III. RESULTS AND DISCUSSION

In this section, I will demonstrate the application of the present WDFT to simple gases represented as LJ fluids near a surface or confined in a slitlike pore. I will also provide some MFT and previous WDFT results for comparisons. To test the present WDFT against molecular simulation data, the fluid-fluid and fluid-solid interactions are the same as those used in the molecular simulations.

A. Density profiles of supercritical fluid near a hard wall or in slitlike pores

The calculated density profiles of the supercritical LJ fluids near a hard wall are compared in Figs. 1–3 with the corresponding computer simulation data[43] at reduced temperature $T^*=k_BT/\varepsilon=1.35$. The external potential for a hard wall can be expressed as

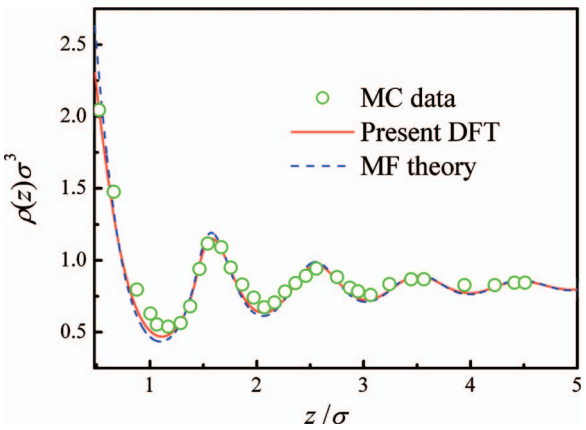

FIG. 3. Same as in Fig. 1 but at a high bulk density of $\rho_b\sigma^3=0.82$.

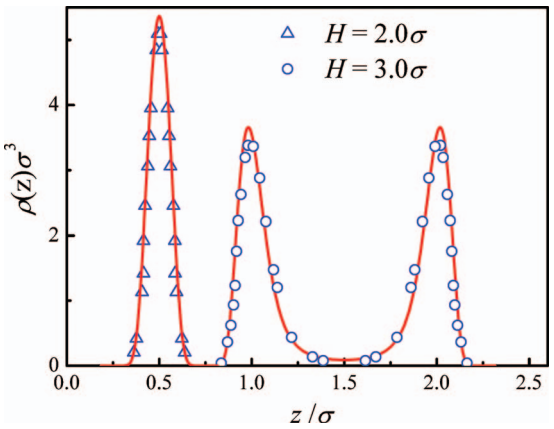

FIG. 4. Density profiles of LJ fluid confined in slitlike pores at bulk density of $\rho_b\sigma^3=0.5925$ and reduced temperature of $T^*=1.2$. The opened triangles and circles represent the GCMC simulation results (Ref. 5) for pore widths of $H=2.0\sigma$ and 3.0σ, respectively. The curves represent the calculated results from the present WDFT. In the calculation, the potential is truncated and shifted at a cutoff distance of $r_c=3.5\sigma$. For clarity, the density profiles for $H=2.0\sigma$ are shifted left by 0.5.

$$\psi^{\text{ext}}(z)=\begin{cases}\infty, & z\le\sigma/2\\ 0, & z>\sigma/2,\end{cases} \tag{29}$$

where $z>0$ is the coordinate in the direction perpendicular to the wall. In the calculation, the attractive part of a truncated and shifted LJ potential in the Barker–Henderson theory is given by

$$u^{\text{att}}(r)=\begin{cases}0, & r\le\sigma\\ u^{\text{LJ}}(r)-u^{\text{LJ}}(r_c), & \sigma<r\le r_c\\ 0, & r>r_c.\end{cases} \tag{30}$$

In Figs. 1–3, both the MFT (i.e., MFMT+MFT) and present WDFT have been applied using the potential given by Eq. (30) with $r_c=5\sigma$. At low density (see Fig. 1 at bulk density $\rho_b\sigma^3=0.5$), the LJ spheres are depleted in the vicinity of the wall and the local density rises monotonically with the increase in the distance from the wall until it reaches the bulk density. The depletion is due to the attraction between the fluid particles, which balances the accumulation of particles due to the short-ranged repulsive interactions. Obviously, the MFT is unable to capture the depletion and is qualitatively incorrect in this case. As the bulk density is increased, the density profiles oscillate around the bulk density indicating that the repulsion is dominant. From Figs. 2 and 3 one can see that the MFT substantially overestimates the oscillation strength. It can be seen from Figs. 1–3 that the present WDFT predicts accurate density profiles of the LJ fluids near the hard wall at all bulk densities when compared to the grand canonical Monte Carlo (GCMC) simulation data.[43]

For a planar slit-pore studied in this work, the external potential can be expressed as

$$\psi^{\text{ext}}(z)=\psi_{sf}(z)+\psi_{sf}(H-z) \tag{31}$$

where $\psi_{sf}(z)$ is the interaction between solid surface and LJ fluid. In Figs. 4, 5, and 9–11, it is given by

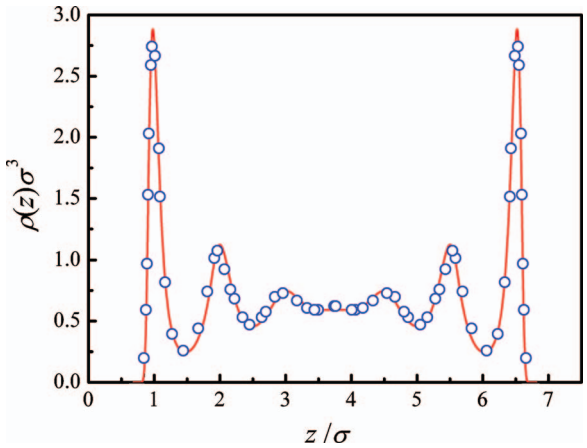

FIG. 5. Density profiles of LJ fluid confined in a slitlike pore with width of $H=7.5\sigma$ at bulk density of $\rho_b\sigma^3=0.5925$ and reduced temperature of $T^*=1.2$. Symbols and solid curve represent the results from the GCMC simulation (Ref. 5) and present WDFT, respectively.

$$\psi_{sf}(z)=\varepsilon_w\left[\frac{2}{5}\left(\frac{\sigma_w}{z}\right)^{10}-\left(\frac{\sigma_w}{z}\right)^4-\frac{\sigma_w^4}{3\Delta(z+0.61\Delta)^3}\right]. \tag{32}$$

In Eq. (32), the values of the wall parameters are $\Delta=\sigma/\sqrt{2}$, $\sigma_w=\sigma$, and $\varepsilon_w=2\pi\varepsilon$ in Figs. 4 and 5, and $\Delta=0.8044\sigma$, $\sigma_w=0.903\sigma$, and $\varepsilon_w=12.96\varepsilon$ in Figs. 9, 11, and 12.

Figures 4 and 5 depict the density profiles of the LJ fluids confined in the slitlike pores with pore widths of $H=2.0\sigma$, 3.0σ, and 7.5σ at bulk density of $\rho_b\sigma^3=0.5925$ and temperature of $T^*=1.2$. Here the LJ potential is truncated and shifted at a cutoff distance of $r_c=3.5\sigma$. Both figures show that the density profiles predicted from the present WDFT is in excellent agreement with the computer simulation data.[5] When the pore becomes very narrow, the fluid in the slitlike pore behaves like a two-dimensional fluid. In this case, if a DFT cannot reduce to the two-dimensional case, its performance will be bad in narrow pores.[10] From Fig. 4 one can see that the present WDFT accurately reproduces the density profile in the very narrow pore (e.g., $H=2.0\sigma$), indicating that the present theory possesses good dimension crossover.

B. Adsorption isotherms of simple gases in the graphitic slit pores

The adsorption of supercritical gases in porous carbons is an important process in gas storage and gas separation. In this subsection, the adsorption isotherms of several simple gases (Ar, N_2, CH_4, and C_2H_6) predicted from the present WDFT are validated against the corresponding simulation data at various pore sizes. The present WDFT is also compared to the nonlocal density functional theory (NLDFT)[17,44] which is frequently used for description of adsorption isotherms in literature.

Nguyen *et al.*[17] simulated simple gases such as argon, nitrogen, and methane in the slit pores with various sizes. In their simulation, the simple gases are modeled by an LJ potential truncated at a cutoff distance of $r_c=1.5$ nm. The LJ parameters used in the simulations and present WDFT calculations are given in Table I. The pore walls contain a single

TABLE I. Parameters of fluid-fluid and fluid-carbon wall interactions (Ref. 17).

Gas	σ (nm)	ε/k_B (K)	σ_{cf} (nm)	ε_{cf}/k_B (K)
Ar	0.3400	119.0	0.3400	57.723
N_2	0.3655	93.98	0.35375	51.298
CH_4	0.3751	148.0	0.357 55	64.374
Ne	0.2820	32.80	···	31.700

carbon plane, and the interaction potential between the single carbon wall and the gas molecule is expressed as

$$\psi_{sf}(z) = 2\pi\rho_c\sigma_{cf}^2\varepsilon_{cf}\left[\frac{2}{5}\left(\frac{\sigma_{cf}}{z}\right)^{10} - \left(\frac{\sigma_{cf}}{z}\right)^4\right], \tag{33}$$

where $\rho_c = 38.17$ atoms nm^{-2} is the number of carbon atoms per unit area in a single graphene layer, corresponding to graphite. The fluid-wall interaction parameters σ_{cf} and ε_{cf} are obtained by the Lorentz–Berthelot combining rules applied to each LJ site of the fluid. Their values used in the GCMC simulations and present WDFT calculations are also listed in Table I.

Figures 6–8 depict the comparisons of adsorption isotherms predicted from the present WDFT with the corresponding GCMC simulation results at 298 K for argon, nitrogen, and methane, respectively. Here the silt-pore walls contain a single carbon plane and the adsorption quantity Γ is defined as

$$\Gamma = \int_0^H \rho(z)dz. \tag{34}$$

For comparison, the adsorption isotherms of the three simple gases on slit pore from the NLDFT (Refs. 17 and 44) are also included in Figs. 6–8. It should be pointed out that in the calculation of the NLDFT, the used parameter for the simple gases are determined from the fit of the NLDFT equation of state to the experimental data, different from those used in the GCMC simulations shown in Table I. Once the parameters are fitted against the bulk experimental data, the NLDFT is completely predictive for nanopores.[17,44] Even though, the NLDFT approach underestimates the adsorption isotherms of the three gases in the small pores ($H < 0.827$ nm) and at relatively high pressure ($p > 7$ MPa), as can be seen obviously in Figs. 6(a), 7(a), and 8(a). If the parameters which have the same values as those in the GCMC simulations were used, the NLDFT approach would result in significant deviations due to the fact that the NLDFT approach does not yield accurate bulk equation of state. The discrepancy between the NLDFT results and the GCMC simulation data is normally recognized as a consequence of the MF approximation. Apparently, the present WDFT has overcome the discrepancy of the NLDFT approach. It is observed from Figs. 6–8 that the isotherms of the three gases predicted from the present DFT match very well the corresponding simulation results up to 50 MPa in various slit-pore sizes. It is found that FMT and the Tarazona theory have almost the same accuracy for an inhomogeneous hard-sphere fluid. The reason why the present DFT is more

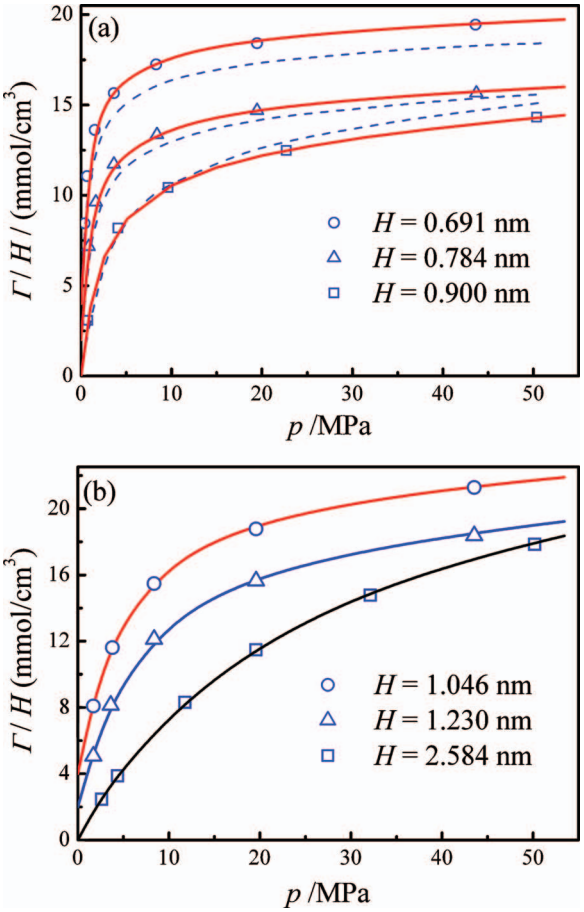

FIG. 6. Comparison of calculated adsorption isotherms of argon with those from the GCMC simulations in the slit pores with various pore widths at 298 K. The pore walls contain a single carbon plane. The symbols, dashed, and solid lines represent the results from the MC simulations (Ref. 17), MFT, and present WDFT, respectively. For clarity, the adsorption isotherms for $H = 0.784$ and 1.230 nm, and $H = 0.691$ and 1.046 nm are shifted upward by 2 and 4, respectively.

accurate than NLDFT of Tarazona, as used by Nguyen *et al.*[17] and Ustinov and Do,[44] is that they neglected the DCF and used a mean-field approximation for the attractive interaction. Compared to existing FMT based DFT, the present WDFT adopts an attractive weighted density to represent the Helmholtz free-energy functional due to the attraction and avoids the DCF as an input. This makes the present WDFT simpler than other existing FMT based DFT without loss of accuracy. Therefore I have not compared the results of the present WDFT with them. If the present WDFT is combined with the finite wall thickness model,[17] the high-pressure adsorption of supercritical gases on activated carbon can be well described.

In Fig. 9, the surface excesses of ethane predicted from the present WDFT are compared to those from the Monte Carlo (MC) simulations in graphitic slit pore at reduced temperature $T^* = 1.35$ and pore widths of $H = 3.5\sigma$ and 5σ. Here ethane is modeled by an LJ potential truncated and shifted at a cutoff distance $r_c = 2.5\sigma$, the fluid-wall interaction is given by Eq. (32) and the surface excess Γ^{ex} of the slit pore is calculated from

$$\Gamma^{ex} = \int_0^H [\rho(z) - \rho_b]dz. \tag{35}$$

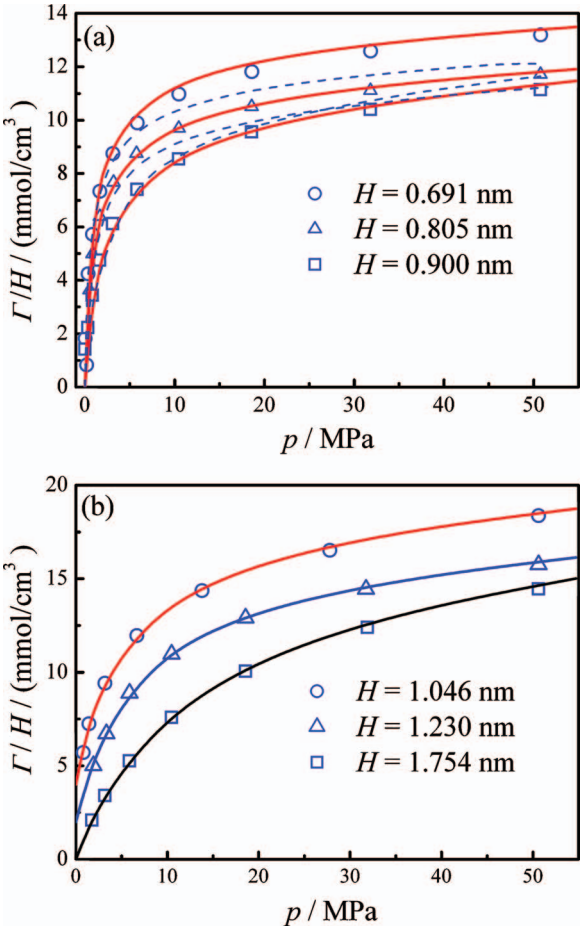

FIG. 7. Comparison of calculated adsorption isotherms of nitrogen with those from the GCMC simulations in the slit pores with various pore widths at 298 K. The pore walls contain a single carbon plane. The symbols, dashed and solid lines represent the results from the MC simulations (Ref. 17), MFT, and present WDFT, respectively. For clarity, the adsorption isotherms in (b) for H=1.230 and 1.046 nm are shifted upward by 2 and 4, respectively.

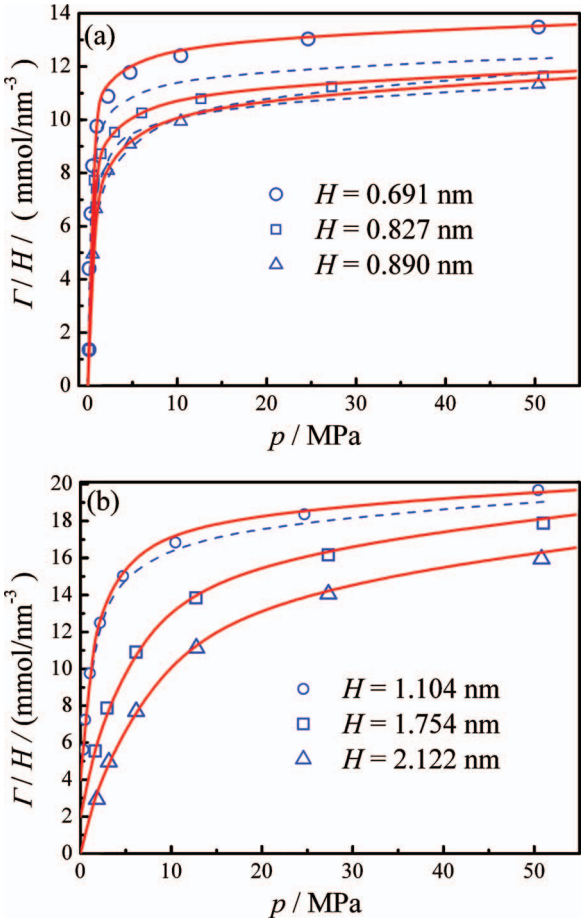

FIG. 8. Comparison of calculated adsorption isotherms of methane with those from the GCMC simulations in the slit pores with various pore widths at 298 K. The pore walls contain a single carbon plane. The symbols, dashed and solid lines represent the results from the MC simulations (Ref. 17), MFT, and present WDFT, respectively. For clarity, the adsorption isotherms in (b) for H=1.754 and 1.104 nm are shifted upward by 2 and 4, respectively.

Figure 9 shows that the present WDFT performs very well for ethane in graphite slit pores. The present WDFT predicts the maximum characteristics of the supercritical surface excess as a function of reduced bulk density in both pore widths. The surface excesses predicted from the present WDFT are in very good agreement with those from the GCMC simulations reported in literature.[32,45] Although the WDFT of Sweatman[32] also gives good description of the surface excesses of ethane in slitlike pores, the weight function used in the present WDFT is much simpler and thus is more computationally efficient than that of Sweatman.

C. Comparison of theoretical adsorption isotherm with experiment

In this section, the theoretical adsorption isotherm of nitrogen is compared to the experiment. The present WDFT has been applied to the nitrogen adsorption on the surface of a graphitized carbon black, which is considered as a representative of a crystalline solid.[46,47] The results at 77 K are plotted in Fig. 10. In the calculation, nitrogen is modeled by the LJ potential with $r_c=4\sigma$ and the carbon wall-nitrogen molecule interactions are described by Eq. (32), where $\varepsilon_w=2\pi\rho_{\text{solid}}\sigma_{cf}^2\varepsilon_{cf}\Delta(1-k_{cf})$ with $\rho_{\text{solid}}=114.0$ nm^{-3} and $\Delta=0.335$ nm. To reproduce the experimental adsorption isotherm,[47] the interaction parameter k_{cf} was selected as the only adjustable parameter and its optimized value is $k_{cf}=0.2397$. For comparison, the results from the Brunauer–Emmett–Teller (BET) equation and the semiempirical Dubinin–Kaganer–Radushkevich (DKR) equation[48] are also included in Fig. 10. The present WDFT accurately reproduces the experimental data in the pressure range covering five orders of magnitude. In contrast, the BET equation only yields reasonable estimations in the range of relative nitrogen pressures from 0.08 to 0.3. Figure 10 also shows that DKR equation behaves very poor in description of the adsorption isotherm.

D. Fluid-solid interfacial tension of simple gas in slit pores

Fluid-solid interfacial tension is a very important thermodynamic quantity in the determination of the surface properties. For example, prewetting and capillary condensation transitions on a surface can be determined through the interfacial tension of both the high and the low branches of

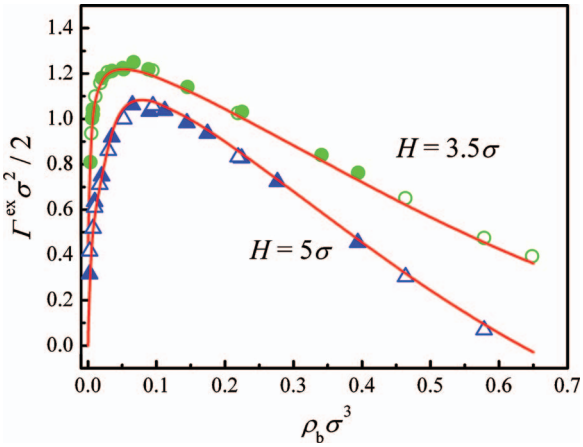

FIG. 9. Comparison of predicted surface excesses of ethane with those from MC simulations in graphitic slit pores at $T^*=1.35$. Ethane is modeled by an LJ potential truncated and shifted at a cutoff distance of $r_c=2.5\sigma$. The opened symbols, solid symbols, and solid lines represent the results from the GCMC simulations of Sweatman (Ref. 32), the GCMC simulations of van Megan and Snook (Ref. 45), and the present WDFT, respectively. For clarity, the results for $H=3.5\sigma$ are shifted upward by 0.4.

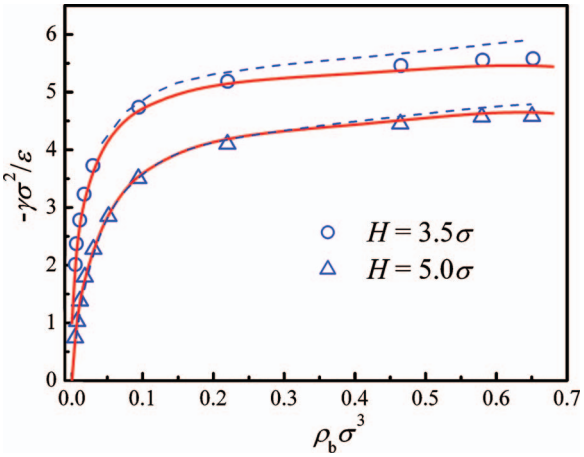

FIG. 11. Comparison of predicted fluid-solid interfacial tensions of ethane with those from GCMC simulations in graphitic slit pores at $T^*=1.35$. Ethane is modeled by an LJ potential truncated and shifted at a cutoff distance of $r_c=2.5\sigma$. The symbols, dashed, and solid lines represent the results from the GCMC simulations, DFT of Sweatman (Ref. 32), and present WDFT, respectively. For clarity, the results for $H=3.5\sigma$ are shifted upward by 1.

the adsorption isotherms.[11,16] The sign of the water-surface interfacial tension is a thermodynamically sound criterion for the "hydrophilicity" or "hydrophobicity" of a surface.[49] The prediction of fluid-solid interfacial tension is a great challenge to the DFTs. It requires that the DFT reproduces an accurate grand potential for the inhomogeneous system under consideration. In this work, the fluid-solid interfacial tension is obtained from the excess grand potential of the inhomogeneous system defined by

$$\gamma=\{\Omega[\rho(z)]-\Omega[\rho_b]\}/A, \tag{36}$$

where A is the area of the interface, and $\Omega[\rho(z)]$ and $\Omega[\rho_b]$ are the grand potentials of the confined fluid in the slitlike pore and the corresponding bulk fluid, respectively. Figure 11 depicts comparisons of predicted fluid-solid interfacial tension of ethane with those from the MC simulations in graphitic slit pores at reduced temperature $T^*=1.35$. Here the fluid-wall interaction is described by Eq. (32). The fluid-solid interfacial tensions of ethane in both pores are negative, indicating that the graphitic walls are strongly "philic" with respect to ethane in these cases. It is easily observed from Fig. 11 that the interfacial tensions from the present WDFT are generally closer to the simulated results than those from the theory of Sweatman.[32] The theory of Sweatman, though is much more complicated than the present WDFT, underestimates the interfacial tensions in both pore widths, especially at high bulk densities. In the theory of Sweatman,[32] the weight function for the attractive contribution is determined from second-order DCF by an *ad hoc* relation. Sweatman employed the hypernetted chain approximation for the Ornstein–Zernike integral[19] equation to generate the second-order DCF. In contrast, our theory avoids the second-order DCF as an input and thus is much simpler than the theory of Sweatman.

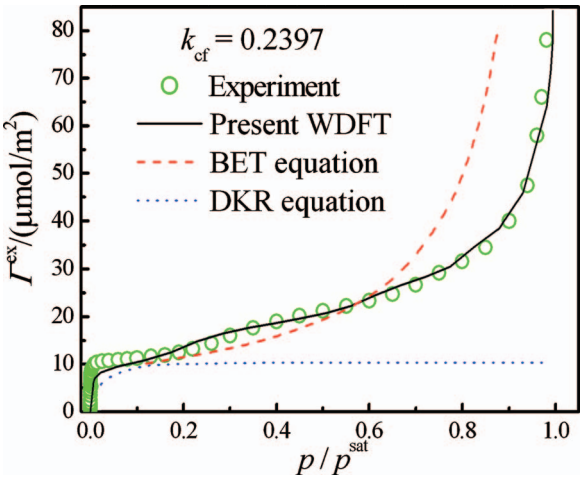

FIG. 10. Comparison between theories and experiment (Ref. 47) for the nitrogen adsorption isotherm on a graphitized carbon black at 77K.

In order to understand how the fluid-surface interaction governs the interfacial tension, I carried out a series of calculations using the present WDFT in which the strength of the fluid-wall potential ε_w and bulk density were varied. The response of the fluid to these variations was analyzed. The calculated results are plotted in Fig. 12, where the slit-pore width is $H=10\sigma$, reduced temperature is $T^*=1.2$, and the wall-fluid potential is given by Eq. (32). It can be seen that the decrease in the potential strength $\varepsilon_w/\varepsilon$ from 4 to 2 changes the sign of the interfacial tension γ and hence makes the wall "phobic" with respect to ethane. When the $\varepsilon_w/\varepsilon > 8$, the walls are strongly philic with respect to ethane. When the wall is phobic, the fluid-solid interfacial tension increases as the bulk density is increased, but when the wall is philic, the interfacial tension changes inversely.

E. Disjoining properties of thin film

The disjoining properties are widely used in modeling thin film phenomena such as wetting, spreading, stability, and evaporation. They have been investigated by experimental measurements[50] and molecular simulations.[2,3] In this work, the equilibrium state of a planar liquid neon film

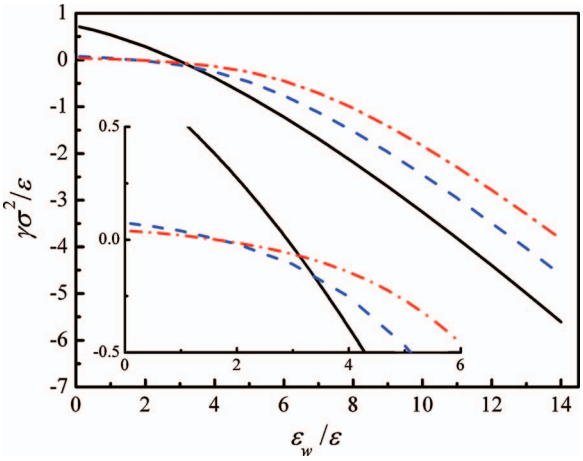

FIG. 12. Predicted fluid-solid interfacial tension of ethane as a function of fluid-wall interaction energy parameter ε_w in a slit pore with pore width of $H=10\sigma$ at bulk densities $\rho_b\sigma^3=0.05$, 0.1, and 0.6, and temperature of $T^*=1.2$. Ethane is modeled by an LJ potential truncated and shifted at a cutoff distance $r_c=2.5\sigma$. Dashed-dotted, dashed, and solid lines represent the results for bulk densities $\rho_b\sigma^3=0.05$, 0.1, and 0.6, respectively.

bounded by vapor and graphitic basal solid plane is investigated using the WDFT proposed in this work. Neon is modeled by an LJ potential truncated and shifted at a cutoff distance $r_c=6.5\sigma$, and the potential parameters are included in Table I. The interaction between neon and graphitic solid surface was described by Steele,[51]

$$\psi^{\text{ext}}(z)=\frac{4\pi\varepsilon_{cf}A^6}{a_s^*}\left[\frac{2A^6}{5}\left(\frac{a_1}{z}\right)^{10}-\left(\frac{a_1}{z}\right)^4-\frac{a_1^4}{3\Delta(z+0.61\Delta)^3}\right], \tag{37}$$

where $a_s^*=\sqrt{3}/2$ is the reduced area of the unit lattice cell, $\Delta=1.38a_1$ is the distance between the discrete planes, $A=1.25$, $a_1=\sqrt{3}\sigma_{ss}$, and $\sigma_{ss}=0.142$ nm is the nearest neighbor distance in the carbon graphitic solid.

When neon gas is absorbed on the carbon graphitic solid surface at temperature T, a film much thinner than the saturated one exists in the vicinity of the surface due to the strong interaction of the film with the basal plane. The disjoining potential is defined as

$$\Delta\mu(h,T)=\mu(h,T)-\mu^{\text{sat}}(T), \tag{38}$$

where $\mu(h,T)$ and $\mu^{\text{sat}}(T)$ are the chemical potentials of the thin film and saturated vapor at temperature T, respectively. The effective film thickness h of the inhomogeneous film is then obtained from the surface excess Γ^{ex},

$$h=\Gamma^{\text{ex}}/(\rho_b^{\text{sat}(L)}-\rho_b^v), \tag{39}$$

where $\rho_b^{\text{sat}(L)}$ and ρ_b^v are the bulk saturated-liquid density and the bulk vapor density, respectively. The disjoining pressure is defined as the difference between the pressure normal to the planar film surface and that of the bulk liquid. In the DFT, it is expressed as

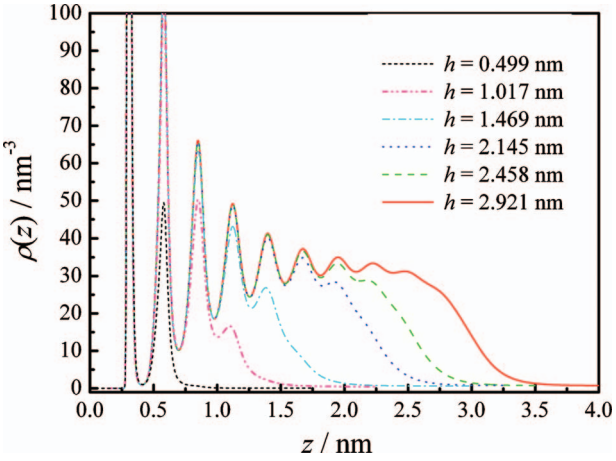

FIG. 13. Density profiles of neon film absorbed on the planar graphite basal plane at 29.52 K. The profiles (from the bottom) correspond to the planar film with effective thicknesses of $h=0.499$, 1.017, 1.469, 2.145, 2.458, and 2.921 nm, respectively.

$$\Pi=-\int_0^\infty dz\rho(z)\left[\frac{\partial\psi^{\text{ext}}(z)}{\partial z}\right]-p_b^L, \tag{40}$$

where p_b^L is the bulk liquid pressure.

Figure 13 depicts the density profiles of the neon film whose effective thickness varies from 0.499 to 2.921 nm at 29.52 K. It can be seen from Fig. 13 that in the vicinity of solid surface (i.e., the interfacial region), the fluid behaves like liquid. The disjoining potential as a function of the effective film thickness h is plotted and compared to the molecular dynamics (MD) simulation data[3] in Fig. 14. Although the accuracy of the MD simulation data is not high, the present WDFT accurately reproduces the simulated disjoining potential, except that it slightly overestimates the disjoining potential at very small film thickness. In this region the disjoining potential decreases very rapidly.

Figure 15 depicts the comparison of the disjoining pressure predicted from the present WDFT with those from the MD simulations. It should be mentioned that the MD simulation data for the disjoining pressure have been recalculated

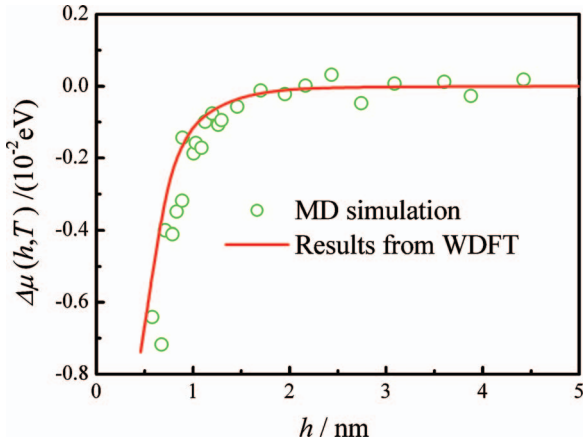

FIG. 14. Disjoining potential as a function of effective film thickness of neon on planar graphite surface at 29.52 K. Neon is modeled by an LJ potential truncated and shifted at a cutoff distance $r_c=6.5\sigma$. Symbols and solid line represent the results from the MD simulations (Ref. 3) and the present WDFT, respectively.

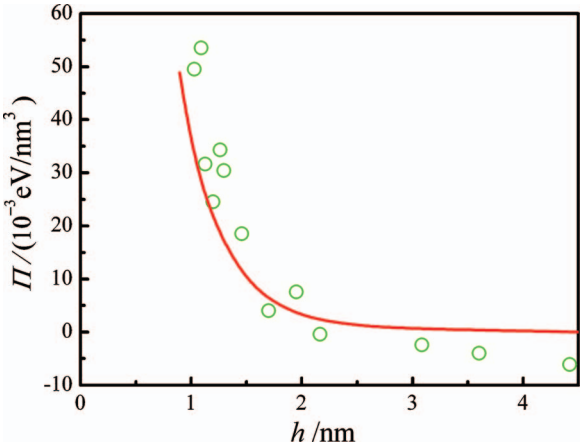

FIG. 15. Disjoining pressure vs the effective film thickness of neon on planar graphite surface at 29.52 K. Symbols and solid line represent the results from the MD simulations (Ref. 3) and the present WDFT, respectively.

from the simulated pressure[3] normal to planar film using the accurate equation of state for the LJ fluid[52] because I found that the disjoining pressure reported by Han is too small. The figure shows that the MD simulation is crude. The variation trend of disjoining pressure is that the disjoining pressure increases slowly as the effective film thickness is decreased to about 2 nm and rises steeply afterward. The present WDFT captures the characteristics of the disjoining pressure and predicts that the disjoining pressure decreases gradually to zero as the film thickness approaches to infinity though the MD simulation data show some degree of fluctuation due to the large simulation errors. Figures 14 and 15 indicate that the present WDFT can be used to predict the disjoining properties of the LJ thin film on the solid surface but the prediction accuracy of the present WDT should be validated by more simulation data. In addition, the use of a more accurate equation of state at low temperature, e.g., the modified Benedict–Webb–Rubin equation of state,[52] could improve the prediction of the present WDFT.

IV. CONCLUSIONS

A novel WDFT is proposed in this work to investigate the density distributions, adsorption isotherms, fluid-solid interfacial tensions, and disjoining properties of simple gases modeled as the LJ fluids in slitlike pores. The LJ potential is separated into repulsive and attractive parts according to the Barker–Henderson perturbation theory.[26] The proposed excess Helmholtz free-energy functional comprises a repulsive contribution from the MFMT of Yu *et al.*,[28,29] an attractive term from the MFT, and a correlation term from the FMSA equation of state with a weighted density. The obtained WDFT is computationally as simple and efficient as the MFT but more accurate. The results predicted from the present WDFT are in excellent agreement with those from the GCMC simulations and experimental results. In addition, the proposed WDFT also performs very well for very narrow pores since it possesses a good dimensional crossover and correctly reduces to the two-dimensional case.

The present WDFT predicts very accurate adsorption isotherms of simple gases such as argon, nitrogen, methane, and ethane in graphitic slitlike pores with various pore sizes. In contrast, the NLDFT approach[17,44] underestimates the adsorption isotherms in the small pores ($H<0.827$ nm) and at relatively high pressures though, the molecular parameters are determined from the fit of the NLDFT equation of state to the experimental data.[44] The discrepancy between the NLDFT results and the GCMC simulation data is due to the MFT approximation and has been overcome by the present WDFT. The fluid-solid interfacial tensions of ethane from the present WDFT are in excellent agreement with those from the GCMC simulations and are better than those from the theory of Sweatman,[32] which slightly underestimates the fluid-solid interfacial tensions at high bulk densities. The present WDFT predicts that the solid wall can be phobic or philic with respect to the fluid by varying the strength of the fluid-wall potential. The decrease in the well depth of the fluid-wall potential may change the sign of interfacial tension and hence may make the wall phobic.

Applications to disjoining properties of neon thin film on the graphitic solid surface show that the present WDFT predicts the disjoining potential and pressure well when compared to the crude MD simulation data.[3] The present WDFT captures all characteristics of the variations of the disjoining potential and pressure as a function of effective film thickness. All the calculated results suggest that the present WDFT is a successful theory for the inhomogeneous LJ fluid. It should be pointed out that the present WDFT is also applicable to other atomic model fluids such as Yukawa, square-well and Sutherland fluids, and thus provides a universal way to construct the excess Helmholtz free-energy functional for inhomogeneous fluids.

ACKNOWLEDGMENTS

The author is very grateful to Dr. Minsub Han for providing the MD simulation data of Fig. 14 and to Dr. Tang for useful discussion of FMSA. This work was supported by the National Natural Science Foundation of China (Grant Nos. 20676065 and 20736003), the Specialized Research Fund for the Doctoral Program of Higher Education (Grant No. 20070003099), and the Program for New Century Excellent Talents in University (NCET) of China.

[1] H. S. Cheng, A. C. Cooper, G. P. Pez, M. K. Kostov, P. Piotrowski, and S. J. Stuart, J. Phys. Chem. B **109**, 3780 (2005); P. G. de Gennes, Rev. Mod. Phys. **57**, 827 (1985).
[2] D. Bhatt, J. Newman, and C. J. Radke, J. Phys. Chem. B **106**, 6529 (2002).
[3] M. Han, Colloids Surf., A **317**, 679 (2008).
[4] E. M. Grzelak and J. R. Errington, J. Chem. Phys. **128**, 014710 (2008); D. D. Do and H. D. Do, *ibid.* **123**, 084701 (2005).
[5] I. K. Snook and W. van Megen, J. Chem. Phys. **72**, 2907 (1980).
[6] P. Szabelski and K. Nieszporek, J. Phys. Chem. B **107**, 12296 (2003); F. Bresme, *ibid.* **106**, 7852 (2002).
[7] R. Evans, Adv. Phys. **28**, 143 (1979).
[8] E. Velasco and P. Tarazona, J. Chem. Phys. **91**, 7916 (1989).
[9] N. Choudhury and S. K. Ghosh, J. Phys. Chem. B **107**, 7155 (2003).
[10] B. Peng and Y.-X. Yu, Langmuir **24**, 12431 (2008).
[11] B. Peng and Y.-X. Yu, J. Phys. Chem. B **112**, 15407 (2008).
[12] Y. P. Tang and J.-Z. Wu, J. Chem. Phys. **119**, 7388 (2003).
[13] D. Fu, J. Chem. Phys. **124**, 164701 (2006).

[14] D. W. Marr and A. P. Gast, Phys. Rev. E **47**, 1212 (1993); I. Napari and A. Laaksonen, J. Chem. Phys. **119**, 10363 (2003); T. X. Nguyen and S. K. Bhatia, J. Phys. Chem. B **108**, 14032 (2004); A. Neimark and P. Ravikovitch, Langmuir **13**, 5148 (1997); D. Henderson, S. Sokolowski, and D. Wasan, Phys. Rev. E **57**, 5539 (1998); L. J. D. Frink and A. G. Salinger, J. Chem. Phys. **118**, 7466 (2003).
[15] F.-Q. You, Y.-X. Yu, and G.-H. Gao, J. Phys. Chem. B **109**, 3512 (2005); Y.-X. Yu, F.-Q. You, Y. Tang, G.-H. Gao, and Y.-G. Li, *ibid.* **110**, 334 (2006).
[16] Y.-X. Yu, G.-H. Gao, and X.-L. Wang, J. Phys. Chem. B **110**, 14418 (2006).
[17] T. X. Nguyen, S. K. Bhatia, and D. Nicholson, Langmuir **21**, 3187 (2005).
[18] R. Evans, in *Fundamentals of Inhomogeneous Fluids*, edited by D. Henderson (Dekker, New York, 1992), pp. 85; H. T. Davis, *Statistical Mechanics of Phases, Interfaces, and Thin Films* (VCH, New York, 1996).
[19] J. P. Hansen and I. R. McDonald, *Theory of Simple Liquids* (Academic, London, 1986).
[20] J. D. van der Waals, Z. Phys. Chem., Stoechiom. Verwandtschaftsl. **13**, 657 (1894).
[21] G. F. Teletzke, L. E. Scriven, and H. T. Davis, J. Chem. Phys. **77**, 5794 (1982); **78**, 1431 (1983).
[22] K. Katsov and J. D. Weeks, J. Phys. Chem. B **105**, 6738 (2001); **106**, 8429 (2002).
[23] D. M. Huang and D. Chandler, J. Phys. Chem. B **106**, 2047 (2002).
[24] Y.-X. Yu, J.-Z. Wu, F.-Q. You, and G.-H. Gao, Chin. Phys. Lett. **22**, 246 (2005); A. Patrykiejew and S. Sokolowski, J. Phys. Chem. B **103**, 4466 (1999); E. Kierlik and M. L. Rosinberg, Phys. Rev. A **44**, 5025 (1991); P. I. Ravikovitch, A. Vishnyakov, and A. V. Neimark, Phys. Rev. E **64**, 011602 (2001).
[25] P. Bryk, S. Bucior, S. Sokolowski, and G. Zukocinski, J. Phys. Chem. B **109**, 2977 (2005); F.-Q. You, Y.-X. Yu, and G.-H. Gao, J. Chem. Phys. **123**, 114705 (2005).
[26] J. A. Barker and D. Henderson, J. Chem. Phys. **47**, 4714 (1967); **47**, 2856 (1967).
[27] J. D. Weeks, D. Chandler, and H. C. Anderson, J. Chem. Phys. **54**, 5237 (1971); B. Q. Lu, R. Evans, and M. M. Telo da Gama, Mol. Phys. **55**, 1319 (1985).
[28] Y.-X. Yu and J. Z. Wu, J. Chem. Phys. **117**, 10156 (2002).
[29] Y.-X. Yu, J. Z. Wu, Y.-X. Xin, and G.-H. Gao, J. Chem. Phys. **121**, 1535 (2004).
[30] R. Roth, R. Evans, A. Lang, and G. Kahl, J. Phys.: Condens. Matter **14**, 12063 (2002).
[31] C. Ebner, W. F. Saam, and D. Strond, Phys. Rev. A **14**, 2264 (1976); W. A. Curtin and N. W. Ashcroft, Phys. Rev. Lett. **56**, 2775 (1986).
[32] M. B. Sweatman, Phys. Rev. E **63**, 031102 (2001).
[33] S. Zhou, Chin. Phys. Lett. **106**, 7674 (2002).
[34] Y. Rosenfeld, J. Chem. Phys. **98**, 8126 (1993).
[35] L. Mederos, E. Chacon, G. Navascues, and M. Lombardero, Mol. Phys. **54**, 211 (1985); S. Sokolowski and J. Fischer, J. Chem. Phys. **96**, 5441 (1992).
[36] F. van Swol and J. R. Henderson, Phys. Rev. A **43**, 2932 (1991).
[37] M. Schmidt, Phys. Rev. E **60**, R6291 (1999); **62**, 4976 (2000).
[38] R. Ohnesorge, H. Lowen, and H. Wagner, Phys. Rev. E **50**, 4801 (1994); M. Muller, L. G. MacDowell, and A. Yethiraj, J. Chem. Phys. **118**, 2929 (2003).
[39] T. Boublik, J. Chem. Phys. **53**, 471 (1970); G. A. Mansoori, N. F. Carnahan, K. E. Starling, and T. W. Leland, *ibid.* **54**, 1523 (1971).
[40] Y. Rosenfeld, Phys. Rev. Lett. **63**, 980 (1989); **72**, 3831 (1994).
[41] Y. P. Tang and B. C.-Y. Lu, AIChE J. **43**, 2215 (1997).
[42] R. L. Cotterman, B. J. Schwarz, and J. M. Prausnitz, AIChE J. **32**, 1787 (1986).
[43] C. Balabanic, B. Borstnik, R. Milcic, A. Rubcic, and F. Sokolic, in *Static and Dynamic Properties of Liquids*, edited by M. Davidoviv and A. K. Soper (Springer, Berlin, 1989), Vol. 40, p. 70.
[44] E. A. Ustinov and D. D. Do, Langmuir **19**, 8349 (2003).
[45] W. van Megen and I. K. Snook, Mol. Phys. **54**, 741 (1985).
[46] K. Miura and H. Yanazawa, Carbon **41**, 151 (2003); M. Kruk, Z. J. Li, and M. Jaroniec, Langmuir **15**, 1435 (1999).
[47] A. A. Isirikyan and A. V. Kiselev, J. Phys. Chem. **65**, 601 (1961).
[48] G. M. Kaganer, Dokl. Akad. Nauk SSSR **116**, 603 (1952).
[49] A. J. Pertsin and M. Grunze, J. Chem. Phys. **118**, 8004 (2003).
[50] N. V. Churaev, Adv. Colloid Interface Sci. **103**, 197 (2003).
[51] W. A. Steele, Surf. Sci. **36**, 317 (1973).
[52] J. K. Johnson, J. A. Zollweg, and K. E. Gubbins, Mol. Phys. **78**, 591 (1993).